

Article

Adaptive Global Carbon Monoxide Kinetic Mechanism over Platinum/Alumina Catalysts

Christopher Depcik^{1,*}, Sudarshan Loya¹, Anand Srinivasan¹, Travis Wentworth² and Susan Stagg-Williams²

¹ Department of Mechanical Engineering, University of Kansas, 3138 Learned Hall, 1530 W. 15th Street, Lawrence, KS, USA; E-Mails: skloya31@ku.edu (S.L.); anandsrinivass@gmail.com (A.S.)

² Department of Chemical and Petroleum Engineering, University of Kansas, 4132 Learned Hall, 1530 W. 15th Street, Lawrence, KS, USA; E-Mails: trav.wentworth@gmail.com (T.W.); smwilliams@ku.edu (S.S.-W.)

* Author to whom correspondence should be addressed; E-Mail: depcik@ku.edu; Tel.: +1-785-864-4151; Fax: +1-785-864-5254.

Received: 25 January 2013; in revised form: 25 April 2013 / Accepted: 20 May 2013 /

Published: 29 May 2013

Abstract: Carbon monoxide (CO) oxidation is one of the more widely researched mechanisms given its pertinence across many industrial platforms. Because of this, ample information exists as to the detailed reaction steps in its mechanism. While detailed kinetic mechanisms are more accurate and can be written as a function of catalytic material on the surface, global mechanisms are more widely used because of their computational efficiency advantage. This paper merges the theory behind detailed kinetics into a global kinetic model for the singular CO oxidation reaction while formulating expressions that adapt to catalyst properties on the surface such as dispersion and precious metal loading. Results illustrate that the model is able to predict the light-off and extinction temperatures during a hysteresis experiment as a function of different inlet CO concentrations and precious metal dispersion.

Keywords: adaptive; kinetics; oxidation; detailed; global; carbon monoxide

Nomenclature:

Variable	Description	Units
a	Constant in pre-exponential	$\text{mol m}^{-2} \text{K}^{-1} \text{s}^{-1}$
A	Adsorption pre-exponential	atm^{-1}
A_{Pt}	Area of platinum site	$\text{m}^2 \text{site}^{-1}$
b	Constant	-
c	Solid specific heat or constant in pre-exponential	$\text{J kg}^{-1} \text{K}^{-1}$ or J mol^{-1}
c_p	Constant pressure specific heat	$\text{J kg}^{-1} \text{K}^{-1}$
\bar{C}	Molar species concentration	mol m^{-3}
d	Channel diameter or constant	m or J mol^{-1}
D	Gas diffusivity	$\text{m}^2 \text{s}^{-1}$
E	Activation energy	J mol^{-1}
G_a	Geometric surface area per unit volume	$\text{m}^2 \text{m}^{-3}$
G_{ca}	Catalytic surface area per unit volume	$\text{m}^2 \text{m}^{-3}$
Gz_m	Mass transfer Graetz number	-
Gz_t	Thermal Graetz number	-
h	Planck's constant (6.626069×10^{-34})	J s
\bar{h}	Molar specific enthalpy	J mol^{-1}
h_c	Heat transfer coefficient	$\text{W m}^{-2} \text{K}^{-1}$
ΔH	Heat of adsorption	J mol^{-1}
ΔH^{\ddagger}	Change in enthalpy in transition state theory	J mol^{-1}
k	Reaction kinetics pre-exponential	$\text{mol m}^{-2} \text{s}^{-1}$
k_B	Boltzmann's constant ($1.3806488 \times 10^{-23}$)	J K^{-1}
K	Adsorption equilibrium	atm^{-1}
m_a	Mass of molecule	kg
N_A	Avogadro's number ($6.02214179 \times 10^{23}$)	mol^{-1}
Nu	Nusselt number	-
p	Pressure	atm
Pr	Prandtl number	-
\dot{q}_{amb}	Ambient heat transfer to or from monolith	W m^{-3}
r	Forward or reverse reaction rate	varies
\bar{R}	Molar gaseous reaction rate	$\text{mol m}^{-2} \text{s}^{-1}$
Re	Reynolds number	-
R_u	Universal gas constant	$\text{J mol}^{-1} \text{K}^{-1}$
S	Sticking coefficient	-
S°	Initial sticking coefficient	-
ΔS^{\ddagger}	Change in entropy in transition state theory	$\text{J mol}^{-1} \text{K}^{-1}$
Sc	Schmidt number	-
Sh	Sherwood number	-
t	Time	s
T	Temperature	K
u	Velocity	m s^{-1}
W	Molecular weight	g mol^{-1}
x	Channel (axial) distance	m

Greek Variables:

Variable	Description	Units
α	Thermal diffusion or constant in desorption activation energy	$\text{m}^2 \text{s}^{-1}$ or -
χ	Heat of adsorption variable	J mol^{-1}
δ	Dispersion	-
ε	Void fraction	-
κ	Mass transfer coefficient	m s^{-1}
λ	Thermal conductivity	$\text{W m}^{-1} \text{K}^{-1}$
Γ	Surface site density	sites m^{-2}
μ	Dynamic viscosity	N s m^{-2}
θ	Surface coverage fraction	-
ν	Kinematic viscosity or frequency of collisions	$\text{m}^2 \text{s}^{-1}$ or s^{-1}
ρ	Density	kg m^{-3}
ω	Catalyst weight normalization factor	-
ζ	Heat of adsorption variable	$\text{J mol}^{-1} \text{K}^{-1}$

Subscripts and Superscripts:

Variable	Description	Units
j	Species index number	-
m	Monolith	-
s	Surface species	-

1. Introduction

Catalysts are important in every industry: chemical, petrochemical, oil-refining, pharmaceutical, organic synthesis, fuel-energetic industries, environment protection, and biocatalysis to name just a few. The chemical reactions on the surface of a catalyst are a function of the inlet chemical species, temperature conditions, metal formulation, washcoat material dispersion/size, and its age causing an immeasurable number of kinetic possibilities. In order to obtain the chemical species conversion rates, researchers spend a significant amount of experimental time and expense. Often, the use of models helps reduce the amount of experiments needed. In specific, models can help predict costs, material placement, effectiveness, and ageing among other items. Accurate and predictive models are needed as catalysts are being asked to perform longer at higher levels of effectiveness. With respect to modeling the reactions occurring on the surface, there are two pathways a researcher can take: detailed or global kinetics.

Detailed kinetic mechanisms allow the researcher to write the reactions as a function of the catalyst metal on the surface and permit different catalyst formulations. However, they are limited from a feasibility standpoint. One concern is that they still require calibration to experimental data because the measurement of all intermediate species on the surface is not feasible without significant experimental capabilities. Even if this happens, industrial revision of the surface metals and the ageing of the device may alter the kinetic constants. Moreover, in the literature there may not be a consensus as to all of the detailed steps needed for the model. For example, researchers have postulated around twenty different

mechanistic steps for the relatively simple reaction of carbon monoxide (CO) with oxygen (O₂) [1–25]. In comparison, global kinetics provides a macroscopic viewpoint of the reaction; CO and O₂ enter the catalyst and carbon dioxide (CO₂) leaves. This allows use of a simpler experimental setup when generating data for calibration of reaction rate expressions.

Furthermore, calibration of a detailed mechanism can take longer than a global mechanism because of the increased number of parameters and experimental tests necessary in order to ensure physically based values. Another issue is that catalysts typically consist of a number of different metals on the surface that may require the detailed mechanism to change and additional reactions to account for subsequent interactions (e.g., enhancement of CO oxidation with hydrogen present [7,19,26]). This will necessitate further experimental tests while also increasing the numerical stiffness of the resultant reaction mechanism. Moreover, the influence of catalyst size, shape, and amount make it nearly impossible to determine one set of kinetic constants for one reaction. As a result, creating adaptive global kinetics, that include facets of the detailed mechanism while factoring in metal properties (e.g., dispersion), have the potential to be more predictive without significantly increasing the computational burden.

With respect to the literature, there are relatively few global mechanism efforts that attempt to develop a more analytical set of kinetics that can be applied to different catalyst formulations [27]. Therefore, the goal of this effort is to create a global kinetic mechanism for CO oxidation that predicts the light-off and light-down temperatures as a function of platinum metal dispersion on the surface. This is done in the absence of other species, like H₂, in order to simplify the effort and focus on the fundamentals instead of creating a simulation that acts as a multiple parameter curve-fit. Of importance, CO oxidation is the first step in exhaust aftertreatment devices for internal combustion engines [4], and it is a critical reaction in the production of hydrogen for fuel cell applications [28,29]. Hence, the results generated will be of interest to researchers in both these fields. Moreover, since sintering increases particle size (dispersion decreases) reducing catalyst effectiveness as it ages [30], this model provides a starting point for a more predictive simulation tool suitable for automotive engineers who prefer the global kinetics route over the detailed approach [31]. Furthermore, this effort endeavors to bridge the gap that exists between Mechanical and Chemical Engineers by demonstrating how surface interactions can be incorporated into a global mechanism. Finally, since the model variables are re-calculated before the simulation begins and the global reaction rate expression is the same, no significant increase in computational load occurs. The automotive industry standard one-dimensional monolithic catalyst model utilized by a wide number of researchers provides the basis of the modeling efforts.

2. Catalyst Model

A previous publication by the first author describes the history of the monolithic one-dimensional (1-D) catalyst model employed in this paper [31]. For this model, two phases capture the bulk and surface (washcoat/substrate) components in the channel. The bulk gas species equation is written as:

$$u \frac{\partial \bar{C}_j}{\partial x} = \frac{\kappa_j G_a}{\varepsilon} (\bar{C}_{s,j} - \bar{C}_j) \quad (1)$$

The left hand side of this equation accounts for the advection of species through the channel and the right hand side describes the mass transfer of species from the bulk gas to the surface under the laminar conditions in the channel.

The bulk gas energy equation is written as a function of temperature:

$$\rho c_p u \frac{\partial T}{\partial x} = \frac{h_c G_a}{\varepsilon} (T_m - T) \quad (2)$$

The left hand side of this equation accounts for the propagation of energy through the channel and the right hand side describes the heat transfer between the gas and the surface.

In these equations, calculation of the diffusion and heat transfer coefficients include entrance effects [32,33]:

$$\kappa_j = \frac{Sh_j D_j}{d} \quad \text{and} \quad h_c = \frac{Nu \lambda}{d} \quad (3)$$

For these expressions, Heck came to the conclusion that Nusselt and Sherwood numbers should correspond to constant heat flux conditions up until light-off and then correspond to the constant wall temperature condition afterwards [34,35]. This is because up until light-off, the region is kinetically controlled; hence, the heat flux is relatively low and approximately constant [32]. Since the experiments modeled later in this paper consist of both light-off and extinction data in order to explore the hysteresis effects of CO oxidation, the constant heat flux conditions will be employed during light-off as developed by Groppi *et al.* [32]:

$$Nu = Sh = 3.095 + 8.933 \left[\frac{1000}{Gz} \right]^{-0.5386} \exp \left[-\frac{6.7275}{Gz} \right] \quad (4)$$

with the constant wall temperature conditions employed during the extinction experiments

$$Nu = Sh = 2.977 + 6.854 \left[\frac{1000}{Gz} \right]^{-0.5174} \exp \left[-\frac{42.49}{Gz} \right] \quad (5)$$

where Gz in the above equation represents the respective mass transfer ($Sh \rightarrow Gz_m$) and thermal Graetz ($Nu \rightarrow Gz_t$) numbers that are written as a function of distance from the inlet:

$$Gz_m = \frac{d Re Sc_j}{x} \quad \text{and} \quad Gz_t = \frac{d Re Pr}{x} \quad (6)$$

with

$$Re = \frac{\rho u d}{\mu}, \quad Sc_j = \frac{\mu}{\rho D_j}, \quad \text{and} \quad Pr = \frac{\nu}{\alpha} \quad (7)$$

As commonly accepted, the Chilton-Colburn analogy equates heat and mass transfer for the laminar flow conditions [36,37].

Simulation of chemistry on the surface of the catalyst happens via a combined treatment of gas concentrations within the washcoat:

$$\frac{d\bar{C}_{s,j}}{dt} = \frac{\kappa_j G_a}{1 - \varepsilon} (\bar{C}_j - \bar{C}_{s,j}) - \frac{G_{ca} \bar{R}_j}{1 - \varepsilon} \quad (8)$$

This equation is written as an Ordinary Differential Equation and solved until steady state so the user does not have to incorporate an algebraic-differential solver for the non-linear equations. The first term on the right hand side describes species mass transfer between the bulk gas and surface and the second term indicates the reaction rates of the gases on the surface. The difference in the mass transfer source term between this equation and the bulk gas equation relates to the relative volume difference between the bulk and surface as indicated by the void fraction (ε).

Completing the 1-D model requires the inclusion of the monolith energy equation for the combined washcoat and substrate (e.g., one numerical node) in the direction normal to the flow:

$$\rho_m c_m \frac{\partial T_m}{\partial t} = \lambda_m \frac{\partial^2 T_m}{\partial x^2} + \frac{h_c G_a}{1 - \varepsilon} (T - T_m) + \frac{G_{ca}}{1 - \varepsilon} \sum_{j=1}^{NM} \bar{R}_j \bar{h}_j + \dot{q}_{amb} \quad (9)$$

The left hand side of this equation represents the storage of energy in this combined structure; whereas, the right hand side terms describe conduction, heat transfer between the gas and the surface, energy generated through catalytic reactions, and heat transfer to the ambient, respectively [38]. Since the experiments simulated from the literature in this paper do not include ambient information, the model assumes adiabaticity as commonly accepted and this term is equal to zero.

3. Reaction Kinetics

The authors chose to reduce the complexity of this initial effort by simulating only the carbon monoxide (CO) oxidation reaction over platinum/alumina:



Choice of this reaction allows the authors to calibrate the global reaction expression to available literature experimental data of varying dispersion, particle diameter, and metal weight with similar BET surface area values. The authors have investigated the history of CO oxidation and determined that most researchers believe that the reaction occurs via the following detailed kinetic steps:



CO adsorption is the first step of the mechanism because of the low initial sticking coefficient of oxygen on platinum as compared to CO [39]. The second step in this mechanism is the dissociative adsorption of oxygen [18,40]. Most researchers believe that the final step is that of adsorbed CO interacting with adsorbed atomic oxygen via a Langmuir-Hinshelwood (L-H) mechanism. This appears to be the most widely assumed prospect, but mechanisms developed using only these conversion reactions do not necessarily predict the most accurate results [8,9,13,14]. The final step would be desorption of CO₂ from platinum that most assume happens instantaneously; hence, Equation (11c)

lumps this step into the final detailed reaction. There is still no true consensus as to the Rate-Determining Step (RDS). A number of researchers indicate that both Equation (11b) and Equation (11c) can be the RDS [17,19,41]. It is quite possible that at lower CO concentrations, Equation (11c) is the RDS and at higher CO concentrations, Equation (11b) becomes the RDS. This paper will utilize the RDS equal to Equation (11c) because it has been shown by Wojciechowski and Asprey to accurately fit experimental data [20]. This results in the following global reaction equation:

$$\bar{R}_{\text{CO}} = -\frac{k_{\text{CO}} \exp\left(-\frac{E_{\text{CO}}}{R_u T_m}\right) K_{\text{CO}} K_{\text{O}_2}^{1/2} p_{\text{CO}} p_{\text{O}_2}^{1/2}}{\left(1 + K_{\text{CO}} p_{\text{CO}} + K_{\text{O}_2}^{1/2} p_{\text{O}_2}^{1/2}\right)^2} \quad (12)$$

where the adsorption equilibrium constants are equal to:

$$K_{\text{CO}} = r_a / r_{-a} = A_{\text{CO}} \exp\left(-\frac{\Delta H_{\text{CO}}}{R_u T_m}\right) \quad (13)$$

$$K_{\text{O}_2} = r_b / r_{-b} = A_{\text{O}_2} \exp\left(-\frac{\Delta H_{\text{O}_2}}{R_u T_m}\right) \quad (14)$$

This is the same global mechanism calculated by Hori and Schmidt in 1975 using molecular oxygen adsorption [5] and Goodman *et al.* in 1982 for atomic oxygen [12].

Table 1. Literature values of CO oxidation model.

Parameter (unit)	Values
k_{CO} (atm s ⁻¹)	1.443 × 10 ¹⁶ ; 8.628 × 10 ¹⁵ [20] 6.27 × 10 ⁹ ; 2.04 × 10 ¹⁰ [42]
k_{CO}/R_u (mol K m ⁻³ s ⁻¹)	1.759 × 10 ²⁰ ; 1.051 × 10 ² 7.651 × 10 ¹³ ; 2.486 × 10 ¹⁴
E_{CO} (kJ mol ⁻¹)	146.2; 144.4 [20] 63.9; 63.9 [42]
A_{CO} (atm ⁻¹)	6.832 × 10 ¹ ; 5.306 × 10 ⁻¹ [20] 1.145 × 10 ⁰ ; 1.087 × 10 ⁰ [42]
ΔH_{CO} (kJ mol ⁻¹)	-7.495; -37.13 [20] -18.4; -18.4 [42]
A_{O_2} (atm ⁻¹)	1.991 × 10 ⁻⁶ ; 1.053 × 10 ⁻¹¹ [20] 5.286 × 10 ⁻⁶ ; 8.810 × 10 ⁻⁸ [42]
ΔH_{O_2} (kJ mol ⁻¹)	-82.99; -153.4 [20] 9.3; 9.3 [42]

At this stage, it is possible to calibrate the pre-exponentials, activation energies, and adsorption heats as is often done by researchers. However, as Wojciechowski and Asprey illustrate [20], there can be two different sets of parameters that match the data captured as indicated in Table 1. One issue with kinetics is that it requires collection of a large amount of experimental data in order to eliminate all potential local minimums during parameter optimization. Moreover, since chemical kinetics are non-linear, it is possible to find a set of parameters that matches the data well but may be non-physically based. Hence, the approach the authors take is to explore from first principles the components of the global rate expression in order to minimize the number of variables to calibrate.

3.1. Adsorption Equilibrium Constants

Calculation of the pre-exponential factors for adsorption in Equations (13) and (14) come from kinetic gas theory [43–47]:

$$A_a = \frac{S^0}{(2\pi m_a k_B T_m)^{1/2}} \quad (15)$$

where m_a is the mass of the molecule given by (W/N_A) , N_A is Avogadro's number, W is the molecular weight of the species, k_B is Boltzmann's constant, and S^0 is the sticking coefficient for zero coverage of the species adsorbed. The desorption pre-exponential factor is written as:

$$A_{-a} = \nu_{CO} \Gamma \quad (16)$$

using a rate constant or frequency (ν in units of s^{-1}) determined from theory or experimental studies and the site density of the surface (Γ in sites per m^2). Writing the overall expressions for Arrhenius based adsorption and desorption kinetics via Equation (11a) results in:

$$r_a = A_a e^{-E_a/(R_u T_m)} \quad \text{and} \quad r_{-a} = A_{-a} e^{-E_{-a}/(R_u T_m)} \quad (17)$$

Using Equations (13) and (14) allows for representation of the global rate expressions by combining the results of Equations (15), (16), and (17) into the following example for CO:

$$K_{CO} = \frac{r_a}{r_{-a}} = \frac{S_{CO}^0 \exp[-\Delta H_{CO}/(R_u T_m)]}{\nu_{CO} \Gamma (2\pi m_a R_u T_m)^{1/2}} \quad (18)$$

where the adsorption heats equal $\Delta H_{CO} = E_a - E_{-a}$ and $\Delta H_{O_2} = E_b - E_{-b}$.

Using the site density ($\Gamma = 1/A_{Pt}$) and Boltzmann constant ($k_B = R_u/N_A$) including the area of a Pt site ($A_{Pt} = 8 \times 10^{-20} \text{ m}^2/\text{site}$ [48]) results in expressions as a function of partial pressures:

$$K_{CO} = \frac{N_A A_{Pt} S_{CO}^0}{\nu_{CO} (2\pi W_{CO} R_u T_m)^{1/2}} \exp\left(-\frac{\Delta H_{CO}}{R_u T_m}\right) \quad (19)$$

$$K_{O_2} = \frac{N_A A_{Pt} S_{O_2}^0}{\nu_{O_2} (2\pi W_{O_2} R_u T_m)^{1/2}} \exp\left(-\frac{\Delta H_{O_2}}{R_u T_m}\right) \quad (20)$$

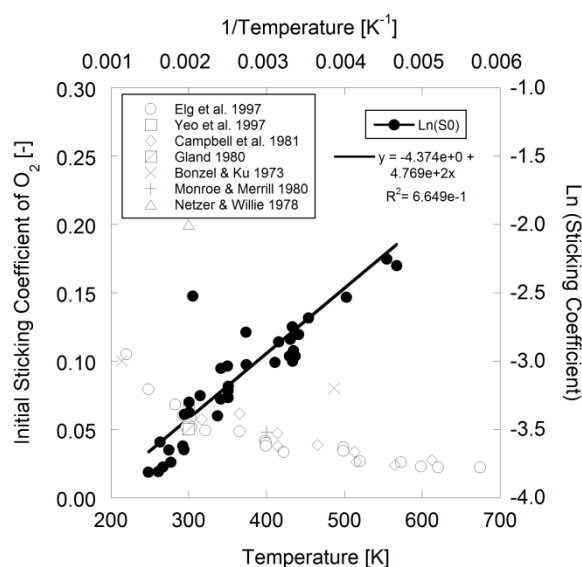
Ideally, one should obtain values for all of these parameters over the same catalyst; however, the literature review that follows demonstrates this is not possible. Therefore, this paper will assume a few values even though the catalysts where this information comes from may not be the same.

3.2. Sticking Coefficients

Sticking coefficients can be a function of surface temperature, the angle of the bond with the gas, and the current coverage of the surface. From kinetic gas theory, the model is interested only in the initial surface coverage at the starting point of experiments or modeling. Later in this paper, the authors will apply the kinetic model to a Pt/ γ - Al_2O_3 surface; however, most surface coverage values in the literature are found using a single crystalline structure in order to understand the interactions on the

surface. In such cases, the authors postulate that one should use data from the most applicable surface. As discussed later, since some calibration of the kinetics will have to occur (as always), this embeds variations according to surface crystal structure within the resulting values. Face Centered Cubic crystalline materials such as Pt have three main vectors (100), (110) and (111), with imperfect or stepped plains predominately represented by Pt₁₁₁ and Pt₁₁₀ vectors. Pt₁₁₁ is a logical choice for physical parameter estimation as it is one of the two dominating crystal plans present in small particle size Pt catalysts [49,50] and will provide the baseline values. This paper will provide data for catalysts when found and may be used if no other option exists.

Figure 1. Sticking coefficient of O₂ over Pt₁₁₁ using data from [11,40,51–55].



With respect to oxygen surface coverage, Elg *et al.* mentions that the temperature dependence of the initial sticking coefficient during dissociative adsorption on Pt₁₁₁ is exponential in nature [40] that Campbell *et al.* wrote as an Arrhenius expression [52]:

$$S_{O_2}^0 = S_{O_2} \exp\left(-\frac{E_{S,O_2}}{R_u T_m}\right) \quad (21)$$

Using available literature data in Figure 1, the authors fit the following parameters to the data for Pt₁₁₁ using Campbell *et al.*'s expression for modeling: $S_{O_2} = 1.260 \times 10^{-2}$ and $E_{S,O_2} = -3.980$ kJ/mol.

For the sticking coefficient of CO, Campbell *et al.* finds that it is angular and temperature independent with a value of 0.84 for Pt₁₁₁ [56]. Yeo *et al.* finds an initial sticking coefficient of 0.80 over Pt₁₁₁ that decreases with CO coverage in monolayers (ML) while mentioning that the initial reactive sticking probability for CO is 0.7 during CO oxidation experiments [51]. Schubert *et al.* [57] mention that standard values for the sticking coefficient of CO range between 0.5 and 0.8. Shigeishi and King determine an initial probability of 0.67 over Pt₁₁₁ [58]. Based on this literature survey, the authors employ a constant initial sticking coefficient of 0.8 for CO as it provides a reasonable approximation of the Pt₁₁₁ values found.

3.3. Heats of Adsorption

With respect to the activation energy of the forward and reverse adsorption steps, Campbell *et al.* indicate that a relatively small value is required for CO to transfer into the chemisorbed state [59]:

$$E_a = 2.5 \text{ kJ/mol} \quad (22)$$

and this value is used for the model.

Table 2. Literature desorption activation energies (E_{-a}) for carbon monoxide.

Value	Catalyst
118–183 [51]	Pt ₁₁₁
120–171 (O-predosed) [60]	Pt ₁₁₀
138–178 [60]	Pt ₁₁₀
146.1 (modulated beam) [56,59]	Pt ₁₁₁
115.1–139 (TDS) [56]	Pt ₁₁₁
147.8 [61]	Pt ₁₁₀
125.6–129.8 (isosteric calculation) [61]	Pt ₁₁₀
100–138.2 [62]	Pt ₁₁₁
117.2 (zero coverage) [63]	Pt ₁₁₁
136.5 [64]	Pt _{100-(5×20)}
171.7–230.3 [65]	Polycrystalline Pt
135 (at saturation) [58]	Pt ₁₁₁

Table 3. Literature desorption activation energies (E_{-b}) for oxygen.

Parameter	Value	Catalyst
E_{-b}	141.6–157.8 [44]	Pt/ γ -Al ₂ O ₃
E_{-b}^0	200 [43]	Pt/ γ -Al ₂ O ₃
α_1	0.115 [43]	Pt/ γ -Al ₂ O ₃
E_{-b}	175.8–213.5 [52]	Pt ₁₁₁
E_{-b}	117.2–213.5 [66]	Pt ₁₁₁
E_{-b}	153–332 [67]	Pt ₁₁₀
E_{-b}	199–335 [60]	Pt ₁₁₀
E_{-b}	125–339 [51]	Pt ₁₁₁
E_{-b}	167 [68]	polycrystalline Pt
E_{-b}	171.7–205.2 [69]	Pt _{(S)-9(111) × (111)}
E_{-b}	154.9 [70]	Pt ₁₁₁
E_{-b}	187.2–290.1 [39]	Pt ₁₀₀
E_{-b}	161.6–216 [64]	Pt _{100-(5 × 20)}
E_{-b}	280.5 [65]	polycrystalline Pt

For oxygen, since it undergoes dissociation as it bonds atomically via Equation (11b), it must overcome a relatively small energy barrier. Olsson *et al.* used the low dispersion data from Holmgren *et al.* over a Pt/Ce catalyst with a value of 21 kJ/mol in their modeling efforts for a gamma-alumina catalyst [71]. For high dispersion, this value equals 0.91 kJ/mol [71]. Gland finds that the dissociative activation energy of oxygen is equal to 29.3 kJ/mol at low oxygen coverage for Pt₁₁₁ [11]. Parker *et al.*

mention that while no determinations of the activation energy for dissociative adsorption of O₂ have been made for > 0.25 ML, the barrier heat can be estimated to be greater than 37.7 kJ/mol from the work of Derry and Ross [66]. They estimate that it should be greater than 79.5 kJ/mol at 0.42 ML, with Derry and Ross illustrating that one should use a value greater than or equal to 67.0 kJ/mol at 0.5 ML of atomic oxygen coverage. Based on the previous discussion regarding differing platinum surfaces, the authors utilize the findings of Gland in this paper for E_b .

When summarizing available literature data for desorption activation energies for carbon monoxide (E_{-a}) and oxygen (E_{-b}) in Table 2 and Table 3, respectively, the results suggest a large range of available values. This range exists because both of these parameters change as a function of the surface coverage of adsorbed species [40,43,66,72–75]. For example, Olsson *et al.* models the activation energy for oxygen desorption in a linear manner with atomic oxygen coverage as:

$$E_{-b} = E_{-b}^0 (1 - \alpha_1 \theta_{\text{Pt-O}}) \quad (23)$$

where $\theta_{\text{Pt-O}}$ is the fractional coverage of the surface by atomic oxygen and α_1 is a constant. This changing activation energy as a function of surface coverage reveals an issue with the global kinetic modeling approach. In such a model, the current state of coverage of the surface is unknown; hence, these activation energies cannot include this option in the model as the reaction proceeds or the inlet concentrations change.

For CO, the authors employ a lumped approach including both the activation energies for adsorption and desorption. In particular, the literature via Table 2 illustrates that the total adsorption heat of this species changes as a function of surface coverage that varies with temperature [72–74]. As a result, the authors model CO adsorption with a temperature dependence:

$$\Delta H_{\text{CO}} = E_a - E_{-a} = \chi + \xi T_m \quad (24)$$

where χ and ξ are calibrated constants. Having χ negative accounts for the desorption heats with the overall value of ΔH_{CO} decreasing (less negative) as a function of temperature. This is because the molecules become more active on the surface and will have an increasing tendency for desorption.

While the heat of desorption of oxygen (E_{-b}) changes with the surface coverage of oxygen, in this effort it is assumed constant and calibrated because of the large value range indicated in Table 3. This assumption stems from the experimental results modeled later. In particular, the oxygen partial pressure is significantly higher as compared to the CO partial pressure (10% O₂ inlet *versus* 0.1% CO). In the kinetically limited region, CO will cover a relatively small part of surface due to its low gas phase concentration despite the higher affinity of CO to platinum. In the mass transfer limited region, this CO will react with surrounding oxygen and leave the surface. However, the surface coverage of oxygen will not change significantly, as only a small amount of CO is available to react relative to the large concentration of oxygen present. Furthermore, given the relatively low concentrations of CO, the surface inhibiting effect of CO is negligible [76]. Moreover, while some oxygen can desorb, the relative rate of desorption is low until about 800 K [40,77]. Since the experiments modeled were accomplished with temperatures lower than 600 K, this should not be an issue. Any small decrease in surface coverage due to desorption will be offset by an increase in coverage area on the newly created free sites due to the reaction.

The authors assume that the adsorption heats are additionally independent of particle size and dispersion. Uner and Uner found in their investigation of initial and integral heats of adsorption that O₂ and CO adsorption processes are not structure sensitive [78]. When consolidating the reaction activation energies measured on these catalysts with the heat of adsorption, they attribute a minor decrease in effective activation energy with increasing particle size to a variation of pre-exponential factors of the elementary reaction steps of the CO oxidation reaction.

3.4. Desorption Rate Constants

The desorption rate constant describes the frequency of the species desorbing from the surface. The literature illustrates a wide range of values for oxygen (ν_{O_2}) for this experimentally determined value as indicated in Table 4. Zhdanov and Kasemo state that one can conclude that the activated complex for adsorption of oxygen, and accordingly for desorption, has rotational and translational degrees of freedom [75]. Hence, this means that this value should be much higher than 10^{13} s^{-1} . Based on this information, the authors follow the efforts of Olsson *et al.* in modeling a Pt/Al₂O₃ catalyst [43] by using their indicated value of 10^{15} s^{-1} .

Table 4. Desorption rate frequencies used or determined in the literature for dissociative oxygen.

Value	Catalyst	Units
1×10^{13} [68]	Pt ₁₁₁	s ⁻¹
1×10^{15} [75]	Pt ₁₁₁	s ⁻¹
2.4×10^{-2}	Pt ₁₁₁	cm ² s ⁻¹ /s ⁻¹
3×10^{13} [52]	Pt ₁₁₁	cm ² s ⁻¹ /s ⁻¹
2.6×10^{-1} [66]	Pt ₁₁₁	NA
1.5×10^{-5} [67]	Pt ₁₁₀	ML s ⁻¹
1×10^{13} [11]	Pt ₁₁₁	s ⁻¹

Table 5. Desorption rate frequencies in the literature for CO.

Value	Catalyst	Units
1.25×10^{15} [56,59]	Pt ₁₁₁	s ⁻¹
6.0×10^{14} [61]	Pt ₁₁₀	s ⁻¹
1×10^{13} [62]	Pt ₁₁₁	s ⁻¹
1×10^{15} [63]	Pt ₁₁₁	s ⁻¹
7.5×10^{12} [64]	Pt _{100-(5×20)}	s ⁻¹

For carbon monoxide (ν_{CO}), Campbell *et al.* mention that the value of the pre-exponential factor derived from modulated beam results is larger than usually expected for first order desorption ($\sim 10^{13}$); other papers find values on the order of 10^{15} s^{-1} or even higher [56] with an indication of values found provided in Table 5. Schubert *et al.* [57] use standard values of 10^{13} to 10^{16} s^{-1} in their effort. Fair and Madix [61] mention that this factor contains the ratio of the single particle partition functions, which are dependent on contributions from electronic translational, rotational and vibrational degrees of freedom. Assuming a value of one for the transmission coefficient, they calculate a value of $9 \times 10^{17} \text{ s}^{-1}$ that they consider as the upper limit. Yeo *et al.* [51] assumes a value of 10^{15} s^{-1} based on the efforts of

Ertl *et al.* [63]. Because of this survey, this work employs a value of 10^{15} s^{-1} since two researchers use this value and it is in the middle range of the limits found.

3.5. Rate Determining Step

Transition state theory relates the rate constant of the Rate Determining Step (RDS) to the equilibrium constant for the transition state that is a function of the Gibbs energy of the transition state. Using the relationship between entropy, enthalpy and Gibbs energy, the reaction rate constant is:

$$k_{\text{CO}} \exp\left(-\frac{E_{\text{CO}}}{R_u T_m}\right) = \frac{k_B T_m}{h} \exp\left(\frac{\Delta S^+}{R_u}\right) \exp\left(-\frac{\Delta H^+}{R_u T_m}\right) \quad (25)$$

where h is Planck's constant and the enthalpy and entropy terms come from the transition state free energy. This expression provides a theoretically based form of the more commonly used Arrhenius equation. In this evaluation, the value for the change in enthalpy, ΔH^+ , is known as the activation energy (E_{CO}) for the particular reaction under study. As a result, writing the k_{CO} component using the transition state theory expression in Equation (25) finds:

$$k_{\text{CO}} = \frac{k_B T_m}{h} \exp\left(\frac{\Delta S^+}{R_u}\right) \quad (26)$$

In this expression, theory indicates that the entropy component is a measure of the degree of order of the intermediate surface reactants. Investigating catalytic properties on the surface, particle size will affect entropy as it changes the nature and bond strength of the components on the surface. In particular, as the particle diameter increases (dispersion decreases), the entropy of the system should decrease as it becomes a less "chaotic" surface leading to a smaller k_{CO} . In other words, larger particles will have larger crystalline faces and fewer instances of defect sites resulting in more organized surface adsorption (e.g., lower entropy). However, as particle diameter decreases, the entropy of the system could possibly increase due to a less uniform surface and more surface defects reducing the organization of the adsorbed species. Furthermore, smaller particle sizes may result in surface stresses due to steric hindrance increasing the surface entropy leading to an increase in k_{CO} [79,80]. While possible, this is only a small dependency and not an overriding factor. Finally, with decreasing dispersion, the frequency of the reaction should decrease (smaller k_{CO}) since there are fewer sites where Pt CO and Pt O are next to each other.

Moreover, catalyst weight will influence the overall reaction rate as it can increase (or decrease) the number of reacting sites. Hence, from a modeling standpoint, the authors express the pre-exponential factor as:

$$k_{\text{CO}} = a T_m \omega \exp(b\delta) \quad (27)$$

where a and b are constants that require calibration and δ is the dispersion of the metal on the surface. This model includes the catalyst weight normalized by the washcoat weight in order to provide a factor of reaction:

$$\omega = \frac{\text{Pt content}}{\text{Amount applied washcoat}} \quad (28)$$

where the authors assume a linear dependency on this factor for this effort in order to simulate an increasing reaction with more platinum given a constant washcoat amount.

Since particle diameter and dispersion are interrelated, including either parameter as a variable effectively captures the other through inference with most researchers presenting dispersion as a distinction between different catalytic loadings [81–83]. If the length of the catalyst is kept constant and the amount of material uniform, dispersion will determine the size of the metal atom on the surface along with the proximity of two metal atoms or sites of adsorption. In addition, the metal particle size may also decide the chemical bond strength between the adsorbate and the adsorbent. For example, Briot *et al.* demonstrate that changes in particle size influence the heat of adsorption, which is a measure of Pt-O bond strength [84]. They suggest that this can affect the reactivity of the absorbed oxygen with the reacting species. Hence, as the particle size decreases given the same number of sites, the chemical bond strength increases which may further hinder the reaction rate as more energy is required to break the bond [80]. Numerous authors support this statement by indicating that the oxidation reaction is a strong function of particle size [22,80,85,86].

Table 6. Literature activation energies for RDS of reaction (E_{CO}).

Value (kJ mol ⁻¹)	Dispersion	Catalyst
55–157 [51]	-	Pt ₁₁₁
100.9 (low O coverage) [59]	-	Pt ₁₁₁
49.0 (high O coverage) [59]	-	Pt ₁₁₁
125 [87]	-	Pt/ α -Al ₂ O ₃
172 [87]	-	Pt/ α -Al ₂ O ₃
55 [88]	29%	Pt/SiO ₂
72 [88]	63%	Pt/SiO ₂
92 [88]	76%	Pt/SiO ₂
96 [89]	4%	Pt/ γ -Al ₂ O ₃
107 [89]	20%	Pt/ γ -Al ₂ O ₃
115 [89]	29%	Pt/ γ -Al ₂ O ₃
120 [89]	63%	Pt/ γ -Al ₂ O ₃

As a result, dispersion plays a large role in predicting the reaction rate expression and the authors chose this parameter as a primary variable of interest for the activation energy. Since as dispersion increases, particle diameter decreases this in turn influences the bond strength. This is similar to Yang *et al.* who wrote the reaction rate expression as a function of particle size and related the results to dispersion [86]. Hence, when ageing of the catalyst occurs through sintering, the dispersion of the catalytic material will change. Note that ageing and sintering can also change the structure of the catalyst particles resulting in different values for the sticking coefficients, activation energies, and heats of adsorption.

Table 7. Constant parameters of adaptive kinetics model.

Parameter	Value	Units
A_{Pt}	8×10^{-20}	$m^2 \text{ site}^{-1}$
N_A	6.022142×10^{23}	molecules mol^{-1}
W_{CO}	28.01	g mol^{-1}
W_{O_2}	31.9988	g mol^{-1}
R_u	8.314472	$\text{J mol}^{-1} \text{ K}^{-1}$
S_{CO}	0.8	-
E_b	29.3	kJ mol^{-1}
ν_{O_2}	1×10^{15}	s^{-1}
ν_{CO}	1×10^{15}	s^{-1}

In regards to the activation energy, Oran and Uner found a large variation in values over different surfaces and dispersion values as indicated in Table 6 [90]. Moreover, theory dictates that since the pre-exponential is temperature dependent, the expression for activation energy must also be temperature dependent [91]. From the two-parameter Kooij equation including this dispersion dependency, the activation energy equals:

$$E_{CO} = c\delta + d + R_u T_m \quad (29)$$

where c and d are constants calibrated to the experimental data. The choice of the growth in activation energy as a function of dispersion follows the earlier discussion involving bond strength increasing as a function of growing dispersion. Moreover, a linear model was chosen since this is the simplest version of this dependency to calibrate. This concludes the model development with Table 7 providing the parameters of the model based on the literature study beyond those left for calibration (*i.e.*, a , b , c , d , χ and ξ).

4. Results and Discussion

Calibration of the parameters utilized CO oxidation literature data from a 2005 paper by Arnby *et al.* [23] where the amount of platinum, dispersion, and particle diameter changed between different catalysts as indicated in Table 8. The platinum dispersion and surface area of Arnby *et al.* were calculated from the amount of adsorbed CO, determined by CO chemisorption measurements. The nomenclature relating to the percentage Al_2O_3 (1, 10, and 100%) indicates their preparations methods where they deposit platinum only on part of the available support material. The choice of this paper over their 2004 paper [22] and others for calibration is because both the platinum to washcoat (ω) and BET surface area remains relatively constant between the different catalysts. Therefore, the difference in the data should ideally relate directly to the impact of dispersion and correspondingly the platinum particle size.

Matlab Simulink provided the platform for model calibration by first finding singular values of a , d , and χ that minimized the least-squares curve-fit (LSQ) value between the experimental and simulated temperatures at the 50% CO conversion points over all light-off and extinction tests. The bounds on these parameters came from the respective literature in this area; specifically, Table 6 for d and Table 2 for χ with E_{-b} set equal to 200 kJ/mol based on Table 3. This initial calibration to their hysteresis

experiments found that the model was unable to match the thermal response from their data. Since they did not include a temperature ramp experiment without chemical reactions, measurement of the amount of heat transfer to the ambient and validation of use of monolith properties from the literature was not possible (e.g., density, thermal conductivity, and specific heat as 1800 kg m^{-3} , $1.5 \text{ W m}^{-1} \text{ K}^{-1}$, and $1020 \text{ J kg}^{-1} \text{ K}^{-1}$ respectively [92]). As a result, the authors included monolith density (ρ_m) as another constant for calibration. Using the initial three calibrated components and a literature value of monolith density, this provided the set of parameters for a final calibration involving all eight parameters (a , b , c , d , χ , ξ , ρ_m , and E_{-b}) that minimized the LSQ value between temperatures at 50% CO conversion for both light-off and extinction with the final results given in Table 9.

Table 8. Washcoat parameters utilized in CO light-off experiments.

Parameter	Pt(100%)	Pt (10%)	Pt (1%)	Pt (100%)	Pt (10%)	Pt (1%)
	Al ₂ O ₃ [22]	Al ₂ O ₃ [22]	Al ₂ O ₃ [22]	Al ₂ O ₃ [23]	Al ₂ O ₃ [23]	Al ₂ O ₃ [23]
Pt content/mg	0.30	0.39	0.59	0.52	0.52	0.50
Washcoat/g	0.15	0.20	0.30	0.26	0.26	0.25
Pt/Washcoat/-	0.00200	0.00195	0.00197	0.00200	0.00200	0.00200
Dispersion/%	48	41	26	56	44	21
Mean Pt diameter/nm	2.3	2.7	4.5	2.0	2.6	5.6
BET/m ² /g _{wsh}	151	152	162	160	163	163

Table 9. Final model variables calibrated to Arnby *et al.* 2005 experimental data.

Variable	Value	Units
a	5.703×10^{11}	$\text{mol m}^{-3} \text{ K}^{-1} \text{ s}^{-1}$
b	3.099	-
c	43.254	kJ mol^{-1}
d	83.442	kJ mol^{-1}
χ	-149.185	kJ mol^{-1}
ξ	4.982×10^{-2}	$\text{kJ mol}^{-1} \text{ K}^{-1}$
ρ_m	3380.435	kg m^{-3}
E_{-b}	197.725	kJ mol^{-1}

Figure 2. Calibrated model results in comparison to Arnby *et al.* 2005 experimental data.

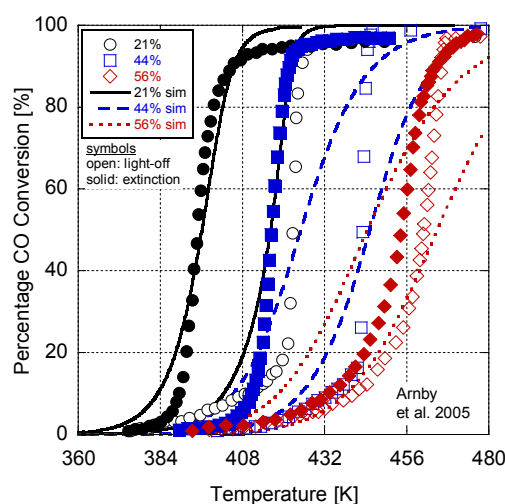


Table 10. Comparison of Root Mean Square Error differences between experimental and simulation conversion percentages (light off/extinction).

Dispersion	Figure 2	Dispersion	Figure 4 (0.01%)	Figure 4 (0.1%)	Figure 4 (1%)
21%	24.1/8.5	26%	47.5/36.4	45.4/20.2	69.7/39.9
44%	21.3/27.8	41%	42.6/32.2	33.6/31.0	62.8/35.9
56%	18.1/14.5	48%	33.5/27.0	21.4/31.8	66.7/45.5

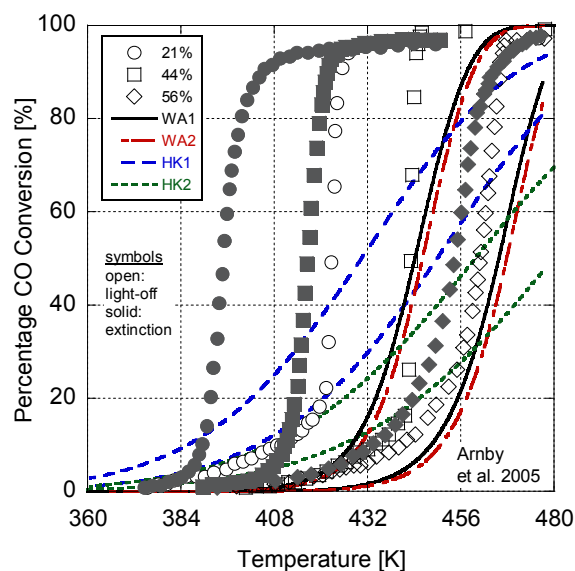
In Figure 2, the model results are presented in comparison to the experimental data. Overall, the model deviates by an average of 5.3K between the 50% conversion points for the light-off and extinction temperatures. In Table 10, a comparison of the Root Mean Squared Error (RMSE) between the simulation and experimental percentages is given. On average, the RMSE indicates a 20% difference in conversion. In order to explore the choice of constants for the last four parameters in Table 5, a sensitivity analysis similar to Ó Conaire [93] was performed by doubling (or halving) the respective value and finding the difference in the 50% light-off and extinction conversion temperatures. Taking the absolute values of the differences, halving S_{CO} was found to change the temperatures by an average of 6.6 K. When doubling E_b , ν_{O_2} , and ν_{CO} , the differences were 20.0, 6.6, and 1.9 K respectively. With respect to the coefficients of Table 9, all model values fall within the respective literature bounds; e.g., at 400K, $\Delta H_{CO} = -129$ kJ/mol (Table 2), $E_{-b} = 197$ kJ/mol (Table 3), and $E_{CO} = 96-111$ kJ/mol (Table 6). Overall, it can be inferred that the calibrated model provides reasonable quantitative values in comparison to the experiments.

With respect to a qualitative analysis, the model accurately captures the trend of 50% conversion temperature with dispersion. However, the higher dispersion values do illustrate a delayed light-off and extinction temperature. Part of this difference could be due to the relatively high monolith density value found in Table 9 resulting in a reduced thermal response of the monolith. Moreover, some of the deviation between the model and experiments (50% conversion temperatures, slope, and RMSE values) relates to the choice of a 1-D model that lumps boundary layer phenomenon into the source terms and washcoat diffusion into the reaction rates. This embeds assumptions into the kinetic parameters reducing the physicality of the model. While it is possible to use more advanced and accurate simulation techniques (e.g., 1 + 1-D model by the authors [94]), this added computational effort made it unfeasible for calibration across all three hysteresis experiments.

Further differences between the results are a function of writing only the pre-exponential and activation energy as a function of dispersion. Metal particle size can influence other parameters, such as the sticking coefficient. This is evident in the difference between the light-off and extinction temperatures. The 56% dispersion experiment only differs by a few degrees Kelvin; however, the 44% and 26% cases are dissimilar by over 30 K. As a result, there is likely some additional non-linearity in the kinetic parameters as a function of dispersion. The results of the sensitivity analysis also demonstrate that the parameters held constant during the analysis might play a role. The authors' endeavored to choose the best values based on the literature in order to reduce the required calibration effort. These may not be the optimum values and may need to be included in the calibration effort. However, the first exploration of a derived dispersion model here warranted the choice of the simplest version in order to explore its practicality. Finally, since the adaptive kinetics only influence the

variables in the reaction rate expression as new values, there is no significant addition to the computational burden of the model while increasing its predictive nature with respect to dispersion.

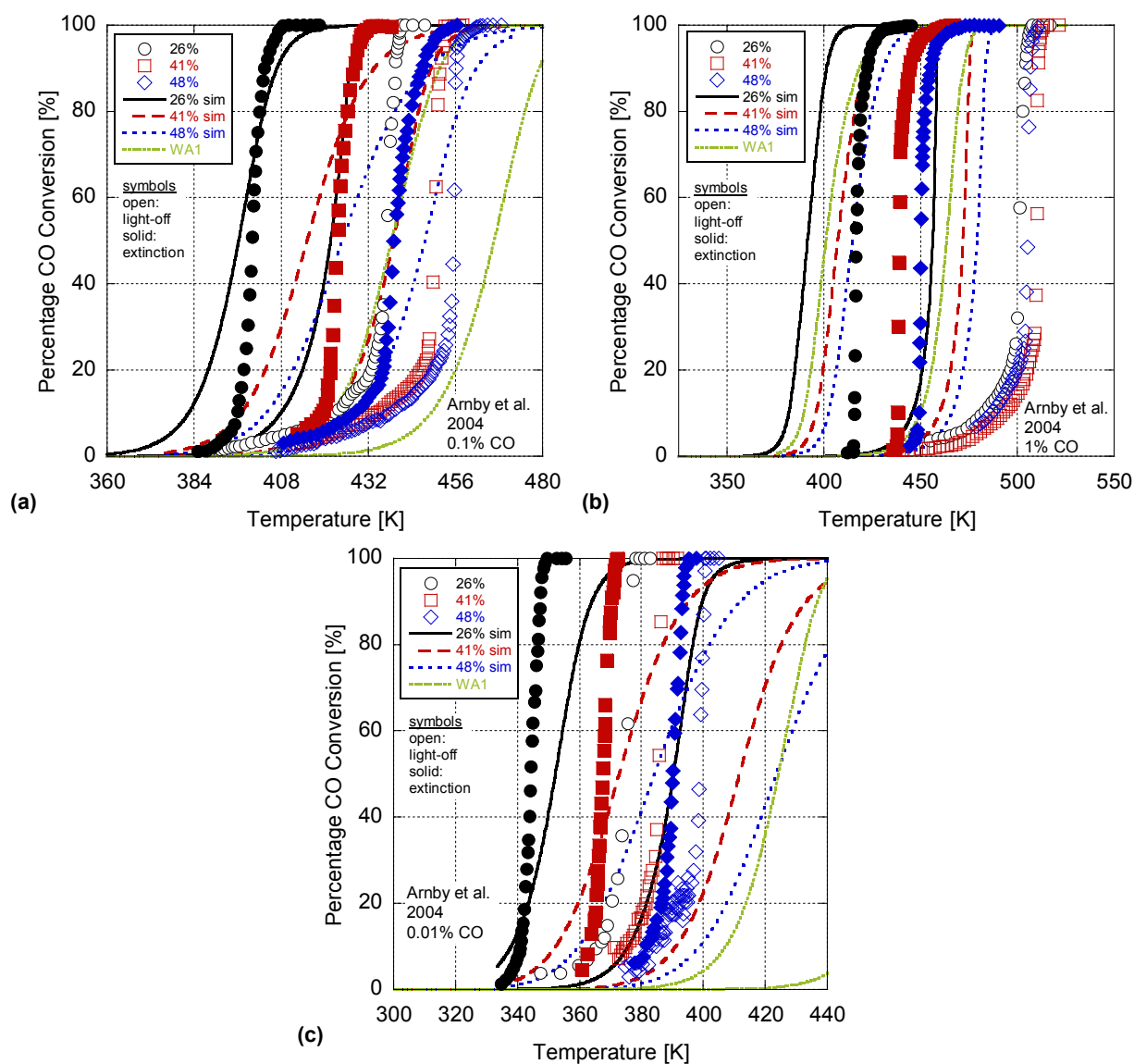
Figure 3. Wojciechowski and Asprey (WA1 and WA2) [20] and Herskowitz and Kenney (HK1 and HK2) [42] model results in comparison to Arnby *et al.* 2005 experimental data.



In order to contrast the derived expressions with models available in the literature, the Arnby *et al.* 2005 experiments were simulated using the four different kinetic options via Wojciechowski and Asprey [20] and Herskowitz and Kenney [42] for the reaction expression of Equation (12) with the coefficients given in Table 1. It is important to note that in order to utilize the pre-exponentials of these authors (k_{CO}) in the same units as this paper required division by the universal gas constant (given in Table 1) that was then divided by the monolith temperature at the time of computation instead of assuming a singular value at all temperatures. Figure 3 illustrates that the Wojciechowski and Asprey models are close to the highest dispersion rate results but significantly deviate from the lowest. Moreover, the Herskowitz and Kenney results do not accurately capture the experimental conditions. It is important to note that these models provide only singular results and cannot depict the influence of surface chemistry.

In order to validate the model, the Arnby *et al.* experiments of 2004 were simulated using the coefficients from Table 9. This 2004 paper utilized three different CO concentration levels; e.g., 0.01%, 0.1%, 1%. Moreover, the catalysts in the 2004 paper had varying Pt content, washcoat mass, and BET surface areas as given in Table 8. Investigating Figure 4, this paper's model accuracy does degrade since it was calibrated to only the 2005 experiments that used 0.1% CO input. In particular, the average deviation between all 50% conversion temperatures increases to 19.3K with the 0.01%, 0.1%, and 1% CO concentration results differing by an average of 14.3K, 10.1K, and 33.5K respectively. Moreover, the RMSE values in Table 10 increase significantly showing a difference of 35, 32, and 55% in conversion percentages. The model does perform best when compared to the 0.1% case since this was the concentration over which the model was calibrated.

Figure 4. Simulation of Arnby *et al.* 2004 (a) 0.1%; (b) 1% and (c) 0.01% CO concentration experiments using the derived kinetics of Table 9 and one set of parameters from Wojciechowski and Asprey.



Moreover, in the Arnby *et al.* 2004 experimental data, they found a deviation in the trend for the 41% dispersion case as it incurred a decreased conversion rate over the 48% dispersion case. The authors theorized that this result may be a function of the relative ratio of Pt to washcoat support which is the lowest of all of the 2004 tests. The model as described in Equation (28) does account for this factor; however, it was unable to be captured by the simulation. Another concern is that for the high CO concentration input (1% CO) the RDS may shift to the oxygen adsorption case via Equation (11b) as discussed in Section 3. This would require a different global reaction mechanism for simulation purposes; hence, the authors' model calibrated to a different RDS would definitely not work. Overall, the model presented here provides the correct trends with dispersion. As dispersion increases, the temperature where light-off and extinction happens, increases. Finally, plotting one Wojciechowski and Asprey value (WA1) set in this figure illustrates that it has the same issue with respect to CO concentration while performing worse at the lowest CO level than the model in this effort. Hence,

while the authors' model does illustrate a significant difference in conversion percentages, its predictability has increased and the methodology for including dispersion in the global rate expression has potential.

While it is indeed possible to recalibrate the model to both the 2004 and 2005 experiments of Arnby *et al.* using Table 9 as the starting parameters, the fact that these experiments include a significant hysteresis effect results in the calibration of reactor heat transfer coefficients alongside the kinetic expression. A common omission from catalyst reactor papers is a reactor warm-up curve or indication that thermal hysteresis was checked during experimentation [2,22–24]. Even with insulated or isothermal reactors, there is still a need to have a temperature rise curve that illustrates the time rate of change of temperature throughout the length of the reactor. This will allow modelers the ability to calibrate the thermal properties (specific heat, density, and thermal conductivity) of the monolith or prove that the kinetic results are not a function of hysteresis. Ideally, just knowing the material of the monolith is sufficient; however, different reactors will have unique thermal conditions and a simple experiment to help modelers eliminate some variability would be significantly helpful. In addition, when experiments contain a large gradient in temperature between the reactor and the ambient, there is a possibility of external heat transfer. A transient heating test of the reactor with the inlet and outlet gas temperatures given as a function of time would help modelers calibrate the associated terms in Equation (9). As a result, spending additional time to calibrate the reaction further was deemed excessive and time was better spent working on setting up a reactor for follow-up experiments.

5. Conclusions

This paper describes an adaptive global kinetics reaction model of CO oxidation over a platinum/alumina catalyst. This model was developed based on the first principles surrounding detailed kinetic mechanisms. A thorough literature search was accomplished in order to minimize the number of constants to calibrate and the results illustrate that the model provides reasonable to good accuracy while capturing the correct dependency on dispersion.

Future work is planned to create a proper Design of Experiments in order to deduce the dependencies as a function of catalyst weight and dispersion. This will provide for better dependencies along with exploration of the different global CO oxidation reaction expressions. As discussed prior, the mechanisms developed using only these conversion reactions do not necessarily predict the most accurate results [8,9,13,14], again illustrating some deviation between the model and experiments. Hence, additional work that provides a better set of data to calibrate the model will shed insight into the adaptive kinetics phenomena. However, this effort illustrates the capability of such a model and demonstrates improved results in comparison to other models available in the literature.

Acknowledgments

This material is based upon work supported by the National Science Foundation under Award No. EPS-0903806 and matching support from the State of Kansas through Kansas Technology Enterprise Corporation.

Conflict of Interest

The authors declare no conflict of interest.

References

1. Hoebink, J.; Nievergeld, A.J.L.; Marin, G.B. CO Oxidation in a Fixed Bed Reactor with High Frequency Cycling of the Feed. *Chem. Eng. Sci.* **1999**, *54*, 4459–4468.
2. Salomons, S.; Hayes, R.E.; Votsmeier, M.; Drochner, A.; Vogel, H.; Malmberg, S.; Gieshoff, J. On the Use of Mechanistic CO Oxidation Models with a Platinum Monolith Catalyst. *Appl. Catal. B* **2007**, *70*, 305–313.
3. Bonzel, H.P.; Ku, R. Carbon Monoxide Oxidation on a Pt(110) Single Crystal Surface. *J. Vacuum Sci. Technol.* **1972**, *9*, 663–667.
4. Voltz, S.E.; Morgan, C.R.; Liederman, D.; Jacob, S.M. Kinetic Study of Carbon Monoxide and Propylene Oxidation on Platinum Catalysts. *Ind. Eng. Chem. Product Res. Dev.* **1973**, *12*, 294–301.
5. Hori, G.K.; Schmidt, L.D. Transient Kinetics in CO Oxidation on Platinum. *J. Catal.* **1975**, *38*, 335–350.
6. Hegedus, L.L.; Oh, S.H.; Baron, K. Multiple Steady States in an Isothermal Integral Reactor: The Catalytic Oxidation of Carbon Monoxide over Platinum-Alumina. *AIChE J.* **1977**, *23*, 632–642.
7. Dabill, D.W.; Gentry, S.J.; Holland, H.B.; Jones, A. The Oxidation of Hydrogen and Carbon Monoxide Mixtures Over Platinum. *J. Catal.* **1978**, *53*, 164–167.
8. Cant, N.W.; Hicks, P.; Lennon, B. Steady State Oxidation of Carbon Monoxide over Supported Noble Metals with Particular Reference to Platinum. *J. Catal.* **1978**, *54*, 372–383.
9. Herz, R.K.; Marin, S.P. Surface Chemistry Models of Carbon Monoxide Oxidation on Supported Platinum Catalysts. *J. Catal.* **1980**, *65*, 281–296.
10. Cutlip, M.B. Concentration Forcing of Catalytic Surface Rate Processes. *AIChE J.* **1979**, *25*, 502–508.
11. Gland, J.L. Molecular and Atomic Adsorption of Oxygen on the Pt(111) and Pt(S)–12(111) x (111) Surfaces. *Surface Sci.* **1980**, *93*, 487–514.
12. Goodman, M.G.; Cutlip, M.B.; Kenney, C.N.; Morton, W.; Mukesh, D. Transient Studies of Carbon-Monoxide Oxidation over Platinum Catalyst. *Surface Sci.* **1982**, *120*, L453–L460.
13. Su, E.; Rothschild, W.G.; Yao, H. CO Oxidation over Platinum/Alumina under High Pressure. *J. Catal.* **1989**, *65*, 281–296.
14. Skoglundh, M.; Lowendahl, L.; Ottersted, J. Combination of Platinum and Palladium on Alumina Supports as Oxidation Catalysts. *Appl. Catal.* **1991**, *77*, 9–20.
15. Nibbelke, R.H.; Nievergeld, A.J.L.; Hoebink, J.H.B.J.; Marin, G.B. Development of a Transient Kinetic Model for the CO Oxidation by O₂ over a Pt/Rh/CeO₂/γ-Al₂O₃ Three-way Catalyst. *Appl. Catal. B* **1998**, *19*, 245–259.
16. Nibbelke, R.H.; Campman, M.A.J.; Hoebink, J.H.B.J.; Marin, G.B. Kinetic Study of the CO Oxidation over Pt/γ-Al₂O₃ and Pt/Rh/CeO₂/γ-Al₂O₃ in the Presence of H₂O and CO₂. *J. Catal.* **1997**, *171*, 358–373.

17. Nijhuis, T.; Makkee, M.; Langeveld, A.; Moulijn, J. New Insight in Platinum Catalyzed CO Oxidation Kinetic Mechanism by Using an Advanced Tap Reactor System. *Appl. Catal.* **1997**, *4*, 237–249.
18. Tieber, W.; Athenstaedt, W.; Leisch, M. SD-Atom-Probe Study of Oxygen-Adsorption on Stepped Platinum Surfaces. *Fresenius J. Anal. Chem.* **1997**, *1–2*, 116–118.
19. Kahlich, M.J.; Gasteiger, H.A.; Behm, R.J. Kinetics of the Selective CO Oxidation in H₂-Rich Gas on Pt/Al₂O₃. *J. Catal.* **1997**, *171*, 93–105.
20. Wojciechowski, B.W.; Asprey, S.P. Kinetic Studies Using Temperature-scanning: The Oxidation of Carbon Monoxide. *Appl. Catal. A* **2000**, *190*, 1–24.
21. Carlsson, P.-A.; Thormählen, P.; Skoglundh, M.; Persson, H.; Fridell, E.; Jobson, E.; Andersson, B. Periodic Control for Improved Low-temperature Catalytic Activity. *Top. Catal.* **2001**, *16/17*, 343–347.
22. Arnby, K.; Törncrena, A.; Andersson, B.; Skoglundh, M. Investigation of Pt/ γ -Al₂O₃ Catalysts with Locally High Pt Concentrations for Oxidation of CO at Low Temperatures. *J. Catal.* **2004**, *221*, 252–261.
23. Arnby, K.; Assiks, J.; Carlsson, P.-A.; Palmqvist, A.; Skoglundh, M. The Effect of Platinum Distribution in Monolithic Catalysts on the Oxidation of CO and Hydrocarbons. *J. Catal.* **2005**, *233*, 176–185.
24. Petersson, M.; Jonsson, D.; Persson, H.; Cruise, N.; Andersson, B. Ozone Promoted Carbon monoxide Oxidation on Platinum/ γ -Alumina Catalyst. *J. Catal.* **2006**, *238*, 321–329.
25. Bourane, A.; Bianchi, D. Oxidation of CO on A Pt/Al₂O₃ Catalyst: From the Surface Elementary Steps to Light-Off Tests-V. Experimental and Kinetic Model for Light-Off Tests in Excess of O₂. *J. Catal.* **2004**, *222*, 499–510.
26. Kim, D.H.; Lim, M.S. Kinetics of Selective CO Oxidation in Hydrogen-rich Mixtures on Pt/Alumina Catalysts. *Appl. Catal. A* **2002**, *224*, 27–38.
27. Konstantas, G.S.; Stamatelos, A.M. Modelling Three-Way Catalytic Converters: An Effort to Predict the Effect of Precious Metal Loading. *Proc. IMechE Part D* **2007**, *221*, 355–373.
28. Igarashi, H.; Fujino, T.; Watanabe, M. Hydrogen Electro-oxidation on Platinum Catalysts in the Presence of Trace Carbon Monoxide. *J. Electroanal. Chem.* **1995**, *391*, 119–123.
29. Jiang, T.; Mowbray, D.J.; Dobrin, S.; Falsig, H.; Hvolbæk, B.; Bligaard, T.; Nørskov, J.K. Trends in CO Oxidation Rates for Metal Nanoparticles and Close-Packed, Stepped, and Kinked Surfaces. *J. Phys. Chem. C* **2009**, *113*, 10548–10553.
30. Strecker, B.; Depcik, C. Macroscopic Study of Projected Catalytic Converter Requirements. *SAE Int.* **2013**, doi:10.4271/2013-01-1286.
31. Depcik, C.; Assanis, D. One-Dimensional Automotive Catalyst Modeling. *Prog. Energy Combust. Sci.* **2005**, *31*, 308–369.
32. Groppi, G.; Belloli, A.; Tronconi, E.; Forzatti, P. A Comparison of Lumped and Distributed Models of Monolith Catalytic Combustors. *Chem. Eng. Sci.* **1995**, *50*, 2705–2715.
33. Hayes, R.E.; Kolaczkowski, S.T. Mass and Heat Transfer Effects in Catalytic Monolith Reactors. *Chem. Eng. Sci.* **1994**, *49*, 3587–3599.
34. Heck, R.; Wei, J.; Katzer, J.R. Mathematical Modeling of Monolithic Catalysts. *AIChE J.* **1976**, *22*, 477–484.

35. Hayes, R.E.; Kolaczkowski, S.T. A Study of Nusselt and Sherwood Numbers in a Monolith Reactor. *Catal. Today* **1999**, *47*, 295–303.
36. Chilton, T.H.; Colburn, A.P. Mass Transfer (Absorption) Coefficients—Prediction from Data on Heat Transfer and Fluid Friction. *Ind. Eng. Chem.* **1934**, *26*, 1183–1187.
37. Grigull, V.; Tratz, H. Thermischereinlauf in Ausgebildeter Laminarerrohrströmung. *Int. J. Heat Mass Transf.* **1965**, *8*, 669–678.
38. Depcik, C.; Kobiera, A.; Assanis, D. Influence of Density Variation on One-Dimensional Modeling of Exhaust Assisted Catalytic Fuel Reforming. *Heat Transf. Eng.* **2010**, *31*, 1098–1113.
39. Kneringer, G.; Netzer, F.P. Adsorption Studies of Oxygen and Carbon-Monoxide on a Pt(100) Surface. *Surface Sci.* **1975**, *49*, 125–142.
40. Elg, A.P.; Eisert, F.; Rosen, A. The Temperature Dependence of the Initial Sticking Probability of Oxygen on Pt(111) Probed with Second Harmonic Generation. *Surface Sci.* **1997**, *382*, 57–66.
41. Chorkendorff, I.; Niemantsverdriet, J. *Concepts of Modern Catal. Kinetics*; Wiley-VCH: Weinheim, Germany, 2007.
42. Herskowitz, M.; Kenney, C.N. CO Oxidation on Pt Supported Catalysts—Kinetics and Multiple Steady-States. *Can. J. Chem. Eng.* **1983**, *61*, 194–199.
43. Olsson, L.; Persson, H.; Fridell, E.; Skoglundh, M.; Andersson, B. A Kinetic Study of NO Oxidation and NO_x Storage on Pt/Al₂O₃ and Pt/BaO/Al₂O₃. *J. Phys. Chem. B* **2001**, *105*, 6895–6906.
44. Olsson, L.; Westerberg, B.; Persson, H.; Fridell, E.; Skoglundh, M.; Andersson, B. A Kinetic Study of Oxygen Adsorption/Desorption and NO Oxidation over Pt/Al₂O₃ Catalysts. *J. Phys. Chem. B* **1999**, *103*, 10433–10439.
45. Dumesic, J.A.; Rudd, D.F.; Aparicio, L.M.; Rekoske, J.E.; Treviño, A.A. *The Microkinetics of Heterogeneous Catalysis*; American Chemical Society: Washington, DC, USA, 1993.
46. Vannice, A. *Kinetics of Catalytic Reactions*; Springer: New York, NY, USA, 2005.
47. White, M. *Heterogeneous Catalysis*; Prentice Hall: Upper Saddle River, NJ, USA, 1990.
48. Andersson, J.R. *Structure of Metallic Catalysts*; Academic Press: London, UK, 1975.
49. García, G.; Koper, M.T.M. Carbon Monoxide Oxidation on Pt Single Crystal Electrodes: Understanding the Catalysis for Low Temperature Fuel Cells. *ChemPhysChem* **2011**, *12*, 2064–2072.
50. Parkinson, C.R.; Walker, M.; McConville, C.F. Reaction of Atomic Oxygen with a Pt(111) Surface: Chemical and Structural Determination using XPS, CAICISS and LEED. *Surface Sci.* **2003**, *545*, 19–33.
51. Yeo, Y.Y.; Vattuone, L.; King, D.A. Calorimetric Heats for CO and Oxygen Adsorption and for the Catalytic CO Oxidation Reaction on Pt{111}. *J. Chem. Phys.* **1997**, *106*, 392–401.
52. Campbell, C.T.; Ertl, G.; Kuipers, H.; Segner, J. A Molecular-Beam Study of the Adsorption and Desorption of Oxygen from a Pt(111) Surface. *Surface Sci.* **1981**, *107*, 220–236.
53. Netzer, F.P.; Wille, R.A. Adsorption Studies on a Stepped Pt(111) Surface—O₂, CO, C₂H₄, C₂N₂. *Surface Sci.* **1978**, *74*, 547–567.
54. Bonzel, H.P.; Ku, R. On the Kinetics of Oxygen Adsorption on a Pt(111) Surface. *Surface Sci.* **1973**, *40*, 85–101.
55. Monroe, D.R.; Merrill, R.P. Adsorption of Oxygen on Pt(111) and its Reactivity to Hydrogen and Carbon Monoxide. *J. Catal.* **1980**, *65*, 461–469.

56. Campbell, C.T.; Ertl, G.; Kuipers, H.; Segner, J. A Molecular-Beam Investigation of the Interactions of CO with a Pt(111) Surface. *Surface Sci.* **1981**, *107*, 207–219.
57. Schubert, M.M.; Kahlich, M.J.; Gasteiger, H.A.; Behm, R.J. Correlation Between CO Surface Coverage and Selectivity/Kinetics for the Preferential CO Oxidation over Pt/Gamma-Al₂O₃ and Au/Alpha-Fe₂O₃: An *In-Situ* DRIFTS Study. *J. Power Sour.* **1999**, *84*, 175–182.
58. Shigeishi, R.A.; King, D.A. Oxidation of Carbon-Monoxide on Platinum (111)—Reflection-Absorption Infrared Spectroscopy. *Surface Sci.* **1978**, *75*, L397–L400.
59. Campbell, C.T.; Ertl, G.; Kuipers, H.; Segner, J. A Molecular-Beam Study of the Catalytic-Oxidation of CO on a Pt(111) Surface. *J. Chem. Phys.* **1980**, *73*, 5862–5873.
60. Wartnaby, C.E.; Stuck, A.; Yeo, Y.Y.; King, D.A. Calorimetric Measurement of Catalytic Surface-Reaction Heat—CO Oxidation on Pt(110). *J. Chem. Phys.* **1995**, *102*, 1855–1858.
61. Fair, J.; Madix, R.J. Low and High Coverage Determinations of the Rate of Carbon-Monoxide Adsorption and Desorption from Pt(110). *J. Chem. Phys.* **1980**, *73*, 3480–3485.
62. Collins, D.M.; Spicer, W.E. Adsorption of CO, O₂, and H₂ on Pt: 1. Thermal Desorption Spectroscopy Studies. *Surface Sci.* **1977**, *69*, 85–113.
63. Ertl, G.; Neumann, M.; Streit, K.M. Chemisorption of CO on Pt(111) Surface. *Surface Sci.* **1977**, *64*, 393–410.
64. Barteau, M.A.; Ko, E.I.; Madix, R.J. The Adsorption of CO, O₂ and H₂ on Pt_{(100)-(5 × 20)}. *Surface Sci.* **1981**, *102*, 99–117.
65. Wood, B.J.; Endow, N.; Wise, H. Competitive Sorption Kinetics of Oxygen and Carbon Monoxide on Platinum. *J. Catal.* **1970**, *18*, 70–76.
66. Parker, D.H.; Bartram, M.E.; Koel, B.E. Study of High Coverages of Atomic Oxygen on the Pt(111) Surface. *Surface Sci.* **1989**, *217*, 489–510.
67. Wartnaby, C.E.; Stuck, A.; Yee, Y.Y.; King, D.A. Microcalorimetric Heats of Adsorption for CO, NO, and Oxygen on Pt{110}. *J. Phys. Chem* **1996**, *100*, 12483–12488.
68. Morris, M.A.; Bowker, M.; King, D.A. Chapter 1 Kinetics of Adsorption, Desorption and Diffusion at Metal Surfaces. In *Comprehensive Chemical Kinetics*; Bamford, C.H., Ed.; Elsevier: London, UK, 1984; Volume 19, pp. 1–179.
69. Schwaha, K.; Bechtold, E. Adsorption of Oxygen on Stepped Pt(S)–9(111)X(111) Face. *Surface Sci.* **1977**, *65*, 277–286.
70. Gland, J.L.; Sexton, B.A.; Fisher, G.B. Oxygen Interactions with the Pt(111) Surface. *Surface Sci.* **1980**, *95*, 587–602.
71. Holmgren, A.; Duprez, D.; Andersson, B. A Model of Oxygen Transport in Pt/ceria Catalysts from Isotope Exchange. *J. Catal.* **1999**, *182*, 441–448.
72. Bourane, A.; Bianchi, D. Heats of Adsorption of the Linear CO Species on Pt/Alumina Using Infrared Spectroscopy: Impact of Pt Dispersion. *J. Catal.* **2003**, *218*, 447–452.
73. Bourane, A.; Dulaurent, O.; Bianchi, D. Heats of Adsorption of Linear and Multibound Adsorbed CO Species on a Pt/Al₂O₃ Catalyst Using *In Situ* Infrared Spectroscopy under Adsorption Equilibrium. *J. Catal.* **2000**, *196*, 115.
74. Bourane, A.; Dulaurent, O.; Chandes, K.; Bianchi, D. Heats of Adsorption of the Linear CO Species on a Pt/Al₂O₃ Catalyst using FTIR Spectroscopy—Comparison Between TPD and Adsorption Equilibrium Procedures. *Appl. Catal. A* **2001**, *214*, 193.

75. Zhdanov, V.P.; Kasemo, B. Simulation of Oxygen Desorption from Pt(111). *Surface Sci.* **1998**, *415*, 403–410.
76. Ehsasi, M.; Matloch, M.; Frank, O.; Block, J.H.; Christmann, K.; Rys, F.S.; Hirschwald, W. Steady and Nonsteady Rates of Reaction in a Heterogeneously Catalyzed Reaction: Oxidation of CO on Platinum, Experiments and Simulations. *J. Chem. Phys.* **1989**, *91*, 4949–4961.
77. Tieber, W.; Athenstaedt, W.; Leisch, M. 3D Atom Probe Study of Oxygen Adsorption on Stepped Platinum Surfaces. *Fresenius J. Anal. Chem* **1997**, *358*, 116–118.
78. Uner, D.; Uner, M. Adsorption Calorimetry in Supported Catalyst Characterization: Adsorption Structure Sensitivity on Pt/ γ -Al₂O₃. *Thermochim. Acta* **2005**, *434*, 107–112.
79. Yates, J.T. Surface Chemistry at Metallic step Defect Sites. *J. Vac. Sci. Technol. A* **1995**, *13*, 1359–1367.
80. Akubiro, E.; Verykios, X. Dispersion and Support Effects in Carbon Monoxide Oxidation over Platinum. *Appl. Catal.* **1985**, *14*, 215–227.
81. Denton, P.; Giroir-Fendler, A.; Praliaud, H.; Primet, M. Role of the Nature of the Support (Alumina or Silica), of the Support Porosity, and of the Pt Dispersion in the Selective Reduction of NO by Propene under Lean-Burn Conditions. *J. Catal.* **2000**, *189*, 410–420.
82. Olsson, L.; Fridell, E. The Influence of Pt Oxide Formation and Pt Dispersion on the Reactions NO₂ \rightleftharpoons NO + 1/2 O₂ over Pt/Al₂O₃ and Pt/BaO/Al₂O₃. *J. Catal.* **2002**, *210*, 340–353.
83. Yates, D.J.C.; Sinfelt, J.H. The Catalytic Activity of Rhodium in Relation to Its State of Dispersion. *J. Catal.* **1967**, *8*, 348–358.
84. Briot, P.; Auroux, A.; Jones, D.; Primet, M. Effect of Particle Size on the Reactivity of Oxygen-adsorbed Platinum Supported on Alumina. *Appl. Catal.* **1990**, *59*, 141–152.
85. McCarthy, E.; Zahradnik, J.; Kuczynski, G.C.; Carberry, J.J. Some Unique Aspects of CO Oxidation on Supported Pt. *J. Catal.* **1975**, *39*, 29–35.
86. Yang, J.; Tschamber, V.; Habermacher, D.; Garin, F.; Gilot, P. Effect of Sintering on the Catalytic Activity of a Pt Based Catalyst for CO Oxidation: Experiments and Modeling. *Appl. Catal.* **2008**, *83*, 229–239.
87. Zafiris, G.S.; Gorte, R.J. CO Oxidation on Pt Alpha-Al₂O₃(0001)—Evidence for Structure Sensitivity. *J. Catal.* **1993**, *140*, 418–423.
88. Gracia, F.J.; Bollmann, L.; Wolf, E.E.; Miller, J.T.; Kropf, A.J. *In situ* FTIR, EXAFS, and Activity Studies of the Effect of Crystallite Size on Silica-supported Pt Oxidation Catalysts. *J. Catal.* **2003**, *220*, 382–391.
89. Atalik, B.; Uner, D. Structure Sensitivity of Selective CO Oxidation over Pt/ γ -Al₂O₃. *J. Catal.* **2006**, *241*, 268–275.
90. Oran, U.; Uner, D. Mechanisms of CO Oxidation Reaction and Effect of Chlorine Ions on the CO Oxidation Reaction over Pt/CeO₂ and Pt/CeO₂/ γ -Al₂O₃ Catalysts. *Appl. Catal. B* **2004**, *54*, 183–191.
91. Laidler, K.J. *Chemical Kinetics*, 3rd ed.; Benjamin Cummins: New York, NY, USA, 1997.
92. Koltsakis, G.C.; Konstantinidis, P.A.; Stamatelos, A.M. Development and Application Range of Mathematical Models for 3-Way Catalytic Converters. *Appl. Catal. B* **1997**, *12*, 161–191.
93. Ó Conaire, M.; Curran, H.J.; Simmie, J.M.; Pitz, W.J.; Westbrook, C.K. A Comprehensive Modeling Study of Hydrogen Oxidation. *Int. J. Chem. Kinetics* **2004**, *36*, 603–621.

94. Depcik, C.; Srinivasan, A. One + One-Dimensional Modeling of Monolithic Catalytic Converters. *Chem. Eng. Technol.* **2011**, *34*, 1949–1965.

© 2013 by the authors; licensee MDPI, Basel, Switzerland. This article is an open access article distributed under the terms and conditions of the Creative Commons Attribution license (<http://creativecommons.org/licenses/by/3.0/>).